Improved motion-compensated MRI and image processing for mid-position lung radiotherapy

Aart van Bochove, Utrecht University

Abstract—

Introduction. **Cardiorespiratory motion causes large positional uncertainty in radiotherapy of the thoracic and abdominal regions. Respiratory-induced uncertainty reduces when treating in the time-weighted average/mid-position (midP) anatomy. This thesis investigates combining a coarse resolution T2w respiratory-correlated 4D-MRI with a high-resolution end-exhale triggered T2w MRI scan (MVXD), to yield a high-resolution midP. Furthermore, including cardiac triggering during MVXD acquisition is proposed. The quality and feasibility of higher-resolution midP and cardiorespiratory triggered MVXD are assessed.**

Methods & materials. **The respiratory-triggered MVXD and a 4D-MRI were acquired for thirteen patients and two healthy volunteers. MidP images, constructed by warping the 4D-MRI phases to the MVXD scan using deformable image registration, were compared to midPs created conventionally by only using the 4D-MRI. The consistency of the deformable vector fields (DVFs) was assessed using the distance discordance metric (DDM).**

Five healthy volunteers were scanned with a cardiorespiratory-triggered MVXD, where the 1D-navigator was placed on the left ventricle (LV) instead of the liver-lung (LL-)interface. 2D cine-MRI images were used to determine residual motion. Three observers assessed the MVXD image quality.

Results. **When including the MVXD in midP calculations, MidP resolution increased nine-fold, yielding sharper images compared to 4D-only midP-MRI. DDM values increased (8% DDM values > 2 mm to $17\% > 2$ mm), indicating reduced DVF consistency, mostly in areas with pulsatile flow (heart, blood vessels) and ghosting (skin), as expected.**

Using LV-based cardiorespiratory triggering, halved the LL- and LV-motion compared to no triggering. According to observers, changing LL-triggering to LV-triggering caused improved heart sharpness in the MVXD images, while LL-interface sharpness decreased slightly. Average scan time increased from 5:46 to 5:51 min.

Conclusion & Discussion. **Involving MVXD in midP calculations increases midP image quality, but DVF consistency slightly reduces, probably due to contrast differences between the scans. Using cardiorespiratory triggering increases MVXD quality around the heart.**

Including the MVXD scan in midP calculation is feasible and useful, and applying cardiorespiratory triggering can increase MVXD quality.

I. Introduction

CARDIORESPIRATORY motion is a large source of uncertainty for radiotherapy treatments in the thoracic and abdominal regions [1]. To make sure the tumor receives enough dose, radiation margins are relatively large, to account for the respiratory motion, with amplitudes around 10-20 mm and frequencies around 0.1-0.3 Hz, as well as for cardiac motion, with amplitudes around 5 mm and frequencies around 1-2 Hz. This results in higher dose in surrounding organs at risk (OARs). Reducing the uncertainty introduced by respiratory and cardiac motion allows for smaller radiation margins, resulting in less radiation for OARs. Furthermore, cardiorespiratory motion negatively impacts image quality as well. Respiratory resolved 4D imaging can be used to capture respiratory-induced tumor motion. In clinical practice 4D-CT is generally used for this purpose [1, 2].

MRI is also in development for use in radiotherapy planning in the thorax and abdomen. Advantages of MRI over CT are the fact that MRI does not involve ionizing radiation, the better soft-tissue contract of MRI compared to CT, and the flexibility in selecting the imaging plane in MRI [3, 4]. The introduction of MR-linac systems adds new possibilities for MRI imaging, since it allows for imaging and radiation to occur simultaneously [5, 6]. When imaging lung using MRI, usually scans with T_1 and with T_2 weighting are both acquired. T_1 weighted images cover high-signal nodules and masses in the lung, while T_2 weighted images highlight tumour infiltration and lesions or masses with high fluid content [7].

One method to reduce respiratory-induced uncertainty during treatment or scanning, is by treating or scanning while the patient holds their breath. However, this is uncomfortable for patients, and some patients are not able to reliably hold their breath for a long time. Therefore other methods of compensating for respiratory motion should be available as well.

One such a method, which is achievable with the MR-linac, is gating, where the tumor is only irradiated in a specific respiratory phase [8]. However, this method is very time-inefficient, since dose will only be delivered in a small part of the respiratory cycle. Therefore either the applied dose per unit of time should be increased, which brings risks, or the treatment time will be increased dramatically.

The uncertainty can also be reduced by treating in the mid-position anatomy, which is the time-weighted average anatomy. An image in the mid-position anatomy can be obtained using deformable image registration on a respiratory-sorted 4D scan [9–11]. A major drawback of 4D-MRI is its relatively coarse resolution, to maintain realistic scan times. Therefore, a mid-position image which is constructed using 4D-MRI might not be directly suited for delineation. An end-exhale triggered MRI scan can be made with higher resolution in addition, in a shorter time. We propose to combine a 1D-navigator end-exhale triggered MRI scan with a respiratory sorted 4D-MRI to obtain a higher resolution mid-position image.

This end-exhale triggered scan does not correct for cardiac motion, which can be a problem for tumors close to or in the heart [12]. We investigated if the quality of the triggered scan

improved further when using cardiorespiratory triggering. We attempted to realise this by moving the 1D-navigator from the liver-lung interface to the left ventricle-lung interface. Earlier research has shown that such a navigator includes information about both respiratory and cardiac motion [13]. To be able to do this, some additional changes had to be applied to the scan protocol.

In this thesis, two research questions will be addressed.

- Will placing a navigator on the left ventricle lead to cardiorespiratory triggering, and thus result in less motion artefacts and higher image quality, compared to respiratory triggering alone?
- Can we use a combination of 4D-MRI and respiratory triggered MRI to obtain a high quality mid-position MRI?

II. Materials & Methods

An end-exhale triggered scan was combined with a 4D-MRI scan, to construct a high-resolution mid-position image using deformable image registration (DIR). The consistency of this mid-position image was assessed using the Distance Discordance Metric (DDM), while the anatomical plausibility was validated by performing a manual rigid registration from the mid-position images to the 4D-MRI scan. The triggered scan was obtained using a 1D-navigator, which was placed on the liver-lung interface, resulting in respiratory triggering. Next, the trigger setup was changed, allowing for cardiorespiratory triggering, by placing the navigator on the left ventricle. A frequency decomposition of the left ventricular motion was used to verify that this motion contained both a respiratory and a cardiac component. 2D-cine images were used to determine the residual motion, and a questionnaire about the image quality was filled in by 3 observers. Finally, the anatomical plausibility was validated by performing a manual rigid registration from the adapted scan to the 4D-MRI scan. The details of each step are explained in the following sections.

A. MRI scans

1) 4D-MRI: A simultaneous multi-slice (SMS-) accelerated coronal 4D-MRI scan (1.9 $\times$ 4-6 $\times$ 1.9 mm^3) was used [14]. We used the turbo spin echo sequence that resulted in T_2 weighted contrast. In this 4D-MRI scan, two slices, separated by half the field of view (FOV), are acquired simultaneously. The FOV is chosen such that the liver-lung interface is always included in one of the two slices, the navigator slice. After acquiring all slices multiple times, for each navigator slice the location of the lung-liver interface is extracted. This information is used to determine the respiratory phase of the navigator slices. Since the other slices were acquired simultaneously, they are in the same respiratory phase as the corresponding navigator slice. The respiratory cycle is divided into ten phases that account for hysteresis. For sorting the data, amplitude binning is used. Due to the stochastic nature of the acquisition, some slices are not acquired in a certain respiratory phase. In that case interpolation is used. Scan parameters can be found in Table I.

2) MVXD scan: The high-resolution (0.5 $\times$ 0.5 $\times$ 3.5) respiratory triggered MRI scan was a T_2 weighted end-exhale triggered axial FSE MultiVane XD (MVXD) scan, also known under the name PROPELLER MRI (Periodically Rotated Overlapping ParallEL Lines with Enhanced Reconstruction) [15]. This scan uses radial readout. This way the central region of k-space is oversampled, which reduces motion artifacts. The main component of respiratory motion is in craniocaudal (CC) direction. This is the through-plane direction, so it is accounted for by the triggering. Several post-processing steps attempt to resolve in-plane motion as well. A 1D pencil-beam navigator is placed on the liver-lung (LL-)interface to extract respiratory motion information [16], as shown in Fig. 1. The navigator had a diameter of 30 mm and a length of 75 mm. The 1D-navigator signal is repeatedly measured every 200 ms. When the subject is in expiration, the LL-interface is at its most cranial location. Since the 1D-navigator is placed on the liver-lung interface, acquisition of several k-space spokes (shots) starts when the navigator position signal is cranial. This is predicted by the velocity of the navigator signal, to remove effects of baseline drift.

a) Proposed adaptations: We slightly adapted the triggered MVXD scan, to make sure the triggering also involves cardiac motion. To allow for this, the navigator was moved to the left ventricle (LV)-lung interface (Fig. 1). A coronal and a sagittal 2D-cine scan were used to help plan the location of the navigator. An example of a cardiorespiratory signal is shown in Fig. 1.

To be able to use cardiorespiratory triggering, some scan parameters were adapted. As stated before, in the original setup, triggers were based on the velocity of the navigator signal, which is easy with respiratory triggering, since the change from inspiration to expiration and vice versa is a large amplitude change in a relatively large amount of time. In contrast, the cardiac component of the cardiorespiratory navigator signal has small changes in a relatively short amount of time. Therefore, the trigger setup was changed to trigger based on the location of the navigator signal. A navigator position signal directed towards the head (i.e., most cranial) corresponds with a heart in diastole, while a signal directed towards the feet (i.e., most caudal) corresponds with systole. If the LV navigator signal is at its most cranial position, the lungs are in expiration, and the heart is in diastole. Furthermore, we adapted the sequence to acquire a single TSE shot instead of multiple shots immediately after each other, since the cardiac cycle is very short. Because of this high cardiac frequency, the triggering frequency was also increased. This led to a navigator acquisition every 50 ms, after which a 155 ms TSE shot followed if the navigator signal was within the gating window. The cardiorespiratory triggered scan will be referred to as the 'LV-MVXD'. The adaptations can also be applied to a MVXD scan with the navigator placed on the LL-interface, such a scan will be referred to as the 'LL-MVXD'. The non adapted scan will be referred to as the 'original MVXD'.

The general and improved scan settings can be found in Table I.

TABLE I: The scan parameters of the acquired scans.

Scan type	SMS-4D-MRI	MVXD			2D cine	
Acquisition plane	Coronal	Axial			Coronal	
Resolution (mm^3)	1.9 × 4-6 × 1.9	0.5 × 0.5 × 3.5			1.5 × 1.5 × 10	
FOV (mm^3)	457 × 208-312 × 457	500 × 500 × 140			325 × 325 × 10	
T_E (ms)	64	79			1	
T_R (ms)	4021	> 5000			2.15	
Imaging frequency (Hz)	NA	NA			11	
Navigator		Original MVXD	LL-MVXD	LV-MVXD	Non-gated cine	Gated cine
Navigator placement	NA	LL	LL	LV	NA	LV
Sampling frequency	NA	5 Hz	20 Hz	20 Hz	NA	20 Hz
Gating based on	NA	Velocity	Position	Position	NA	Position
Gating window	NA	NA	5 mm	5 mm	NA	3.5 mm

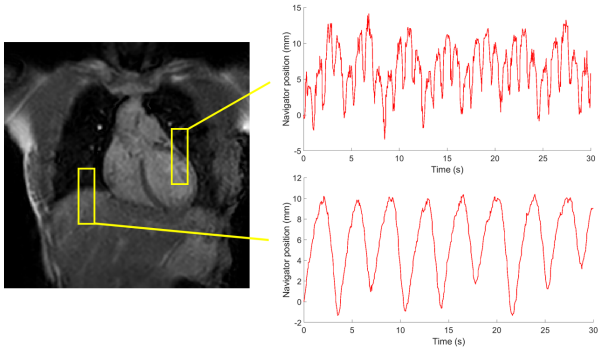

Fig. 1: When placing the navigator on the liver-lung interface, a respiratory signal can be obtained (lower navigator position trace). When placing the navigator on the left ventricle, a cardiorespiratory signal can be obtained (upper navigator position trace).

B. Data acquisition

1) Patients: Thirteen patients (age 42-79, weight 50-100 kg, male:female 9:4) were scanned on a 1.5 T Ingenia MR-sim (Philips Healthcare, Best, The Netherlands). For all patients, an SMS-4D-MRI scan was acquired, as well as a MVXD scan, using the original MVXD. Three other patients were scanned as well, but those datasets were not useful due to a case with large bulk motion, a case with bad gating and a case where only a fat-suppressed MVXD was acquired, which is not used in this research. Patient data was retrospectively collected under the FAST-ART protocol (IRB reference: 20-519/C).

2) Volunteers: Seven healthy volunteers (age 23-37, weight 58-82 kg, male:female 3:4) were scanned on the 1.5 T MR-sim.

For two volunteers, the original MVXD protocol was scanned. A longer version of the SMS-4D-MRI scan was also scanned with these volunteers, to be able to construct multiple 4D-MRI datasets, to make multiple midP images. A total of six 4D-MRI scans could be constructed. Together with the patient scans, these scans were used to evaluate the mid-position imaging.

Five additional healthy volunteers were scanned to assess the LV-MVXD. First, to quantify motion at the LL-interface and LV independently from the navigator, 2D coronal cine images were obtained in three volunteers, covering the projected locations of the LV navigator. Additionally, the heart rhythm of a single volunteer was recorded using peripheral pulse (PPU) during scanning. For three volunteers, 2D cine images were obtained with and without LV gating, to quantify residual motion. For all volunteers, both an LL-MVXD and an LV-MVXD were acquired. Lastly, an SMS-4D-MRI was acquired. Scan parameters for all scans can be found in Table I. Written informed consent was obtained from all healthy volunteers.

C. Evaluation LV-MVXD

The adapted trigger setup was evaluated using the volunteer scans.

1) Frequency decomposition: To demonstrate that the navigator signal contains both a respiratory and a cardiac component when the navigator is placed on the LV, the cine images at the projected locations of the navigator were used. The LV motion, as well as the motion of the LL-interface, in the cine images were extracted using a template matching algorithm using normalized cross-correlation [17]. Prior to template-matching, a 3×3 median filter was applied to the images, and the images were up-sampled with a factor of 2. The size of the crop boxes were around 45×45 mm for the LV motion and around 90×60 mm for the LL-interface motion. A frequency decomposition of the LL- and LV-motion in CC direction, and of the PPU trace was made. These frequency spectra were compared to each other.

2) Residual motion: Residual motion was quantified using the LV-gated and non-gated cine images that were acquired at the same location. The previously described template matching algorithm was used to extract the LV and LL-interface motion in both cine scans. The root mean squared error (RMSE) of the CC-component of the LL- and LV-motion traces in the gated and non-gated cines was compared.

3) Anatomical plausibility: To validate the anatomical plausibility of the LV-MVXD, manual, rigid, translation-only registrations were performed between the MVXD scans and the end-exhale phase of the 4D-MRI. The registration was based on the location of the LL-interface. The MVXD scans should be in end-exhale, so the translation from the MVXD scans to the end-exhale phase of the 4D-MRI should be minimal. The manual registrations were performed with steps of 1 mm, so a precision lower than 1 mm is not expected.

4) Qualitative assessment: The quality of both the LL-MVXD and the LV-MVXD was assessed qualitatively by three observers; one radiologist and two radiation oncologists in

training. They filled in a questionnaire, which asked about the general quality (not usable, bad, okay or good) of the scans and of the different views (axial, coronal and sagittal). They were also asked if certain structures (spine, trachea, bronchus, aorta, heart, esophagus, liver, and the LV-lung interface) were more easy to delineate in one of the two scans, of if there was no difference in that respect. Furthermore, in the axial view, the observers made a slice-by-slice comparison between the two MVXD scans of the quality of the myocardial wall between the LV and the lung, and the esophagus (sharper in one image or in the other). Lastly, the observers were asked about artefacts, and positive and negative properties of the scans. The scans were blinded, meaning that the observers did not know which of the two scans were the LL-MVXD/LV-MVXD. The questionnaire (in Dutch) can be found in Appendix A.

The scan duration of both MVXD scans was evaluated.

D. Mid-position formation

1) 4D mid-position: The mid-position images based solely on the 4D-MRI (4D-midP) are created using the method described by Van de Lindt *et al.* [11]. Fig. 2a shows a schematic overview of this method. To create a midP image, all respiratory phases of a 4D-MRI scan must be registered to a single reference image using DIR. For the 4D-midP, the end-exhale phase is used as a reference image. The calculated deformation vector fields (DVFs) are averaged using a time-weighted average. This DVF represents the DVF from midP to the reference phase. This average DVF can be added to the inverse DVFs, from the reference phase to the other 4D phases, to get DVFs from midP to each separate respiratory phase. These DVFs can be used to warp each phase to the midP anatomy. The final, axially oriented midP is constructed by taking the voxelwise time-weighted median of the resulting warped images. Interpolated data in the 4D-MRI is not used in the final calculation. Time-weighting was based on the relative time spent in each respiratory phase during the acquisition of the 4D-MRI. Because data from multiple 4D-phases are combined into a single midP image, this final image can have a higher resolution ($2 \times 2 \times 2$ mm^3) than the underlying 4D-MRI.

2) MVXD mid-position: A midP with potentially even higher resolution (MVXD-midP) can be calculated by combining the 4D-MRI and the end-exhale triggered MVXD scan. Fig. 2b shows a schematic overview of this method. The method to create a MVXD-midP is very similar to the method described above. Instead of using the end-exhale phase of the 4D-MRI as a reference image, the MVXD image is used. Furthermore, the previously described time-weighted averaged DVF is already enough to warp the MVXD image to midP. The aforementioned inverse registrations, as well as the time-weighted median are not necessary for this procedure. The resolution of the MVXD-midP is equal to that of the MVXD itself ($0.5 \times 0.5 \times 3.5$ mm^3), which is over 9 times higher than that of the 4D-midP.

3) MVXD-based 4D mid-position: To check if the registrations between the 4D-MRI and the MVXD scan can be used to create are reliable midP, a third kind of midP can be constructed (MVXD-4D-midP). Fig. 2c shows a schematic overview of this method. This midP is identical to the 4D-midP, with the exception that the MVXD is used as a reference scan instead of the end-exhale phase of the 4D-MRI. Using the DVFs with the MVXD as a reference, the 4D phases are warped to the midP anatomy. If the registrations with the MVXD scan as a reference can be used to create a reliable midP, this MVXD-4D-midP should be very similar to the 4D-midP.

4) Registration algorithms: The DVFs were calculated using the 'Adaptive (Auto)' module in ADMIRE (Advanced Medical Imaging Registration Engine) Research version 3.35

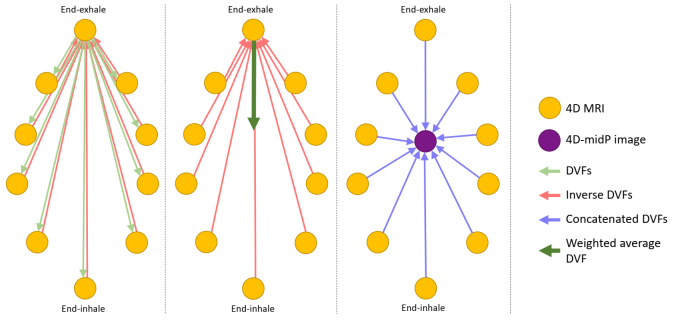

(a) 4D-midP. The DVFs from the 4D-phases to the reference image (the end-exhale phase) can be concatenated with the time-weighted average of the inverse DVFs, to construct a midP, using a time-weighted median.

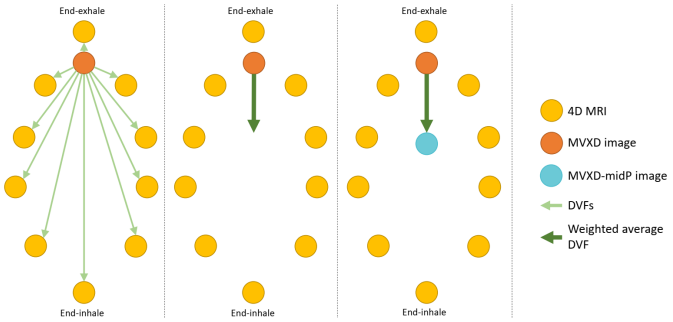

(b) MVXD-midP. The time-weighted average of the DVFs pointing from the MVXD image to each 4D-phase, can be used to warp the MVXD image to the midP.

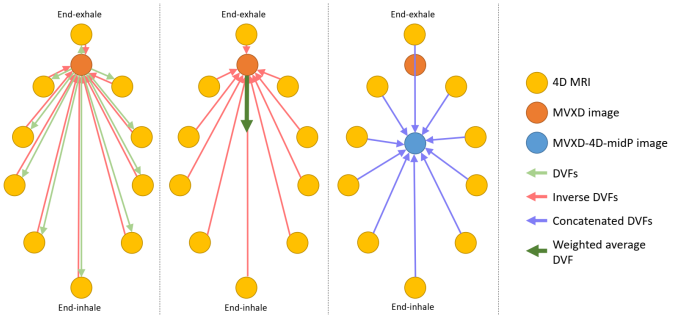

(c) 4D-MVXD-midP. Similar to the 4D-midP formation, except the MVXD image is taken as reference image.

Fig. 2: Visualisation of the methods used to create midP images.

(Elekta AB, Stockholm, Sweden) and using EVolution, with a regularization factor of 0.5 [18]. Results for both algorithms were compared to each other.

E. Evaluation midP

The three types of mid-position images were calculated for all thirteen patients and two healthy volunteers, using the two separate DIR algorithms.

1) DVF consistency: The consistency of the DVFs is quantified using the DDM within the body. The DDM calculations were based on the method by Van de Lindt *et al.* [11], which modified the method of Saleh *et al.* [19]. To calculate the DDM, the DVFs (A) from the end-exhale phase to the end-inhale phase were calculated, via the eight in-between phases. Secondly, DVFs (B) from all individual phases to end-exhale were calculated. The time-weighted average of these DVFs (B) represent the DVF (C) from midP to end-exhale. This DVF (C) can be used to map the previously calculated DVFs (A) to the midP anatomy (D). The DDM can then be calculated by taking the standard deviation of the different DVFs (D) for each voxel. When there is a lot of variation between the registrations, the DDM will be higher, indicating lower DVF consistency. The distribution of DDM values was analysed. The number of DDM values larger than 2 mm was compared to the total number of DDM values, since registration accuracy is desired to be within 2 mm for clinical applications [20]. The spatial distribution of the DDM shows in which sections of the body the registrations are the most consistent.

2) Anatomical plausibility: To validate the anatomical plausibility of the midP images, manual, rigid, translation-only registrations were performed between the midP scans and the end-exhale phase of the 4D-MRI, as well as between all 4D phases to the end-exhale phase of the 4D-MRI. For the volunteers, the registration was based on the location of the LL-interface, while for patients, the tumor was used as a reference structure. Patient data was used only if a clinical GTV delineation was available, if the tumor moved due to respiration, and if the tumor was visible in the 4D-MRI. The data of eight patients could be used, which had nine usable tumors. The registrations between the 4D-MRI phases and the 4D-MRI end-exhale phase were used to calculate the ground-truth translation between the midP to end-exhale. This was compared to the actual translations between the midP images and the end-exhale phase of the 4D-MRI. Ideally the tumor/LL-interface is in the same location in the ground-truth midP (based on the 4D-MRI) as in the actual midPs, resulting in a translation difference of 0 mm. The manual registrations were performed with steps of 1 mm, so a precision lower than 1 mm is not expected.

III. Results

A. Evaluation LV-MVXD

Average (min-max) scan times were 5:46 (4:45-8:02) for the LL-MVXD and 5:51 (3:36-7:18) for the LV-MVXD. Fig. 3 shows example MVXD scans of one volunteer. The left ventricle appears sharper in the LV-MVXD image, compared to the LL-MVXD image. The LL-MVXD shows signal loss in the liver at the location of the navigator.

1) Frequency decomposition: Fig. 5c shows a frequency decomposition of the cardiac motion trace (PPU) of one volunteer. All images in Fig. 5 show a frequency decomposition of the LL-interface and LV motion, based on 2D cine images. For all volunteers, the LL-motion shows a peak around 0.15-0.35 Hz. The cardiac motion shows a clear peak around 1 Hz, and the LV-motion shows peaks around 0.15-0.35 Hz, as well as around 1 Hz.

2) Residual motion: Without triggering, the average (min-max) RSME of LL-interface motion was 3.0 (1.6-4.3) mm in the 2D-cine images, while the RSME of LV motion was 3.8 (2.9-4.3) mm. With LV-triggering, the average (min-max) RSME of LL-interface motion was 1.6 (0.9-2.5) mm, while the RSME of LV motion was 1.9 (1.1-2.4) mm. This means that both types of motion were halved by applying triggering.

3) Anatomical plausibility: Based on the manual registrations, the average (min-max) CC distance between the LL-interface in the MVXD and the end-exhale phase of the 4D-MRI was 0.8 (0.0-2.0) mm for the LL-MVXD, and 1.0 (0.0-2.0) mm for the LV-MVXD, where the LL-interface in the MVXD scans was more caudal (i.e. slightly away from end-expiration).

4) Qualitative assessment: The observers agreed that the general scan quality of the LL-MVXD and the LV-MVXD scans were equal. The image quality of the sagittal plane was scored as not usable to bad, while the coronal view was usually scored as bad. The axial view was almost exclusively scored as okay.

The ability to delineate structures was scored (better in LV-MVXD/LL-MVXD/equal) as follows: The ability to delineate the aorta (2/1/12), oesophagus (3/0/12), spine (0/2/12), liver (4/2/9) and bronchus (2/0/11) was approximately equal, while the heart (9/1/5) was said to usually be easier to delineate in the LV-MVXD. The trachea was outside the field of view in all MVXD scans, and twice the bronchus were said to be outside the field of view.

The LL-interface was scored as being sharper in the LV-MVXD/LL-MVXD/equal (6/8/1) times in the sagittal plane and (4/7/4) times in the coronal plane. For the LV-lung interface, these numbers are (9/6/0) times in the sagittal plane and (6/2/7) times in the coronal plane.

In the axial view, a slice-by-slice comparison of the myocardial wall between the LV and the lung in both scans was performed. For one volunteer, the LL-MVXD was scored higher, with 80%/20% of slices scored as better in the LL-MVXD/LV-MVXD. For the other four volunteers, the LV-MVXD was scored higher, with respectively 27%/71% (one observer forgot one slice, so the numbers do not add up to 100%), 31%/69% 39%/61% and 40%/60% of slices scored as better.The same type of scoring was performed for the esophagus. The observers thought that there was no large difference in the esophagus visibility between the LL-MVXD and the LV-MVXD scans.

In both the LL-MVXD and the LV-MVXD, observers noticed that there were large contrast differences between slices, especially in regions with large motion like the heart and part of the lungs. Both in the LV-MVXD and the LL-MVXD, pulsation artifacts were found in large vessels. A

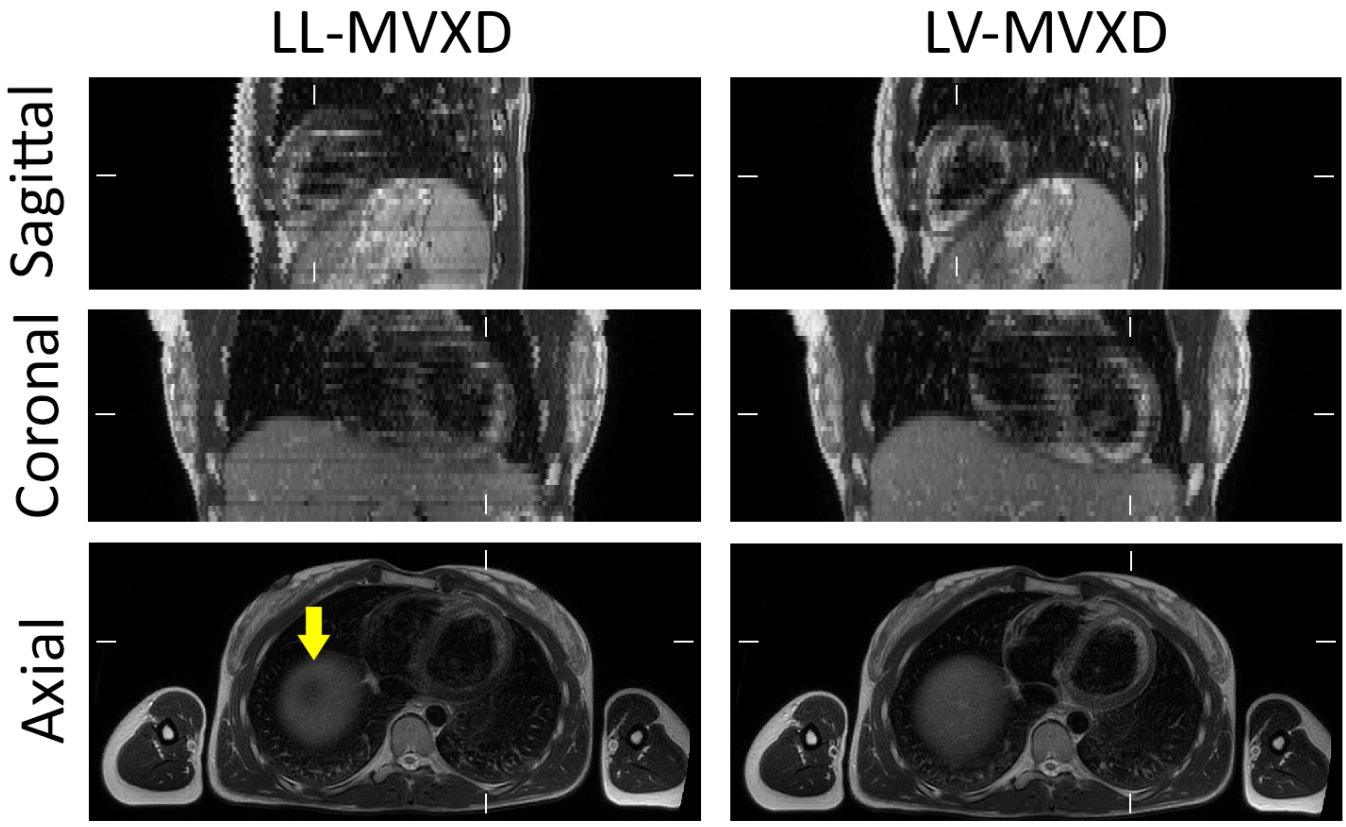

Fig. 3: Here MVXD images for one volunteer is shown. The white ticks show where the planes intersect. The yellow arrow points to a signal void in the liver, caused by the navigator.

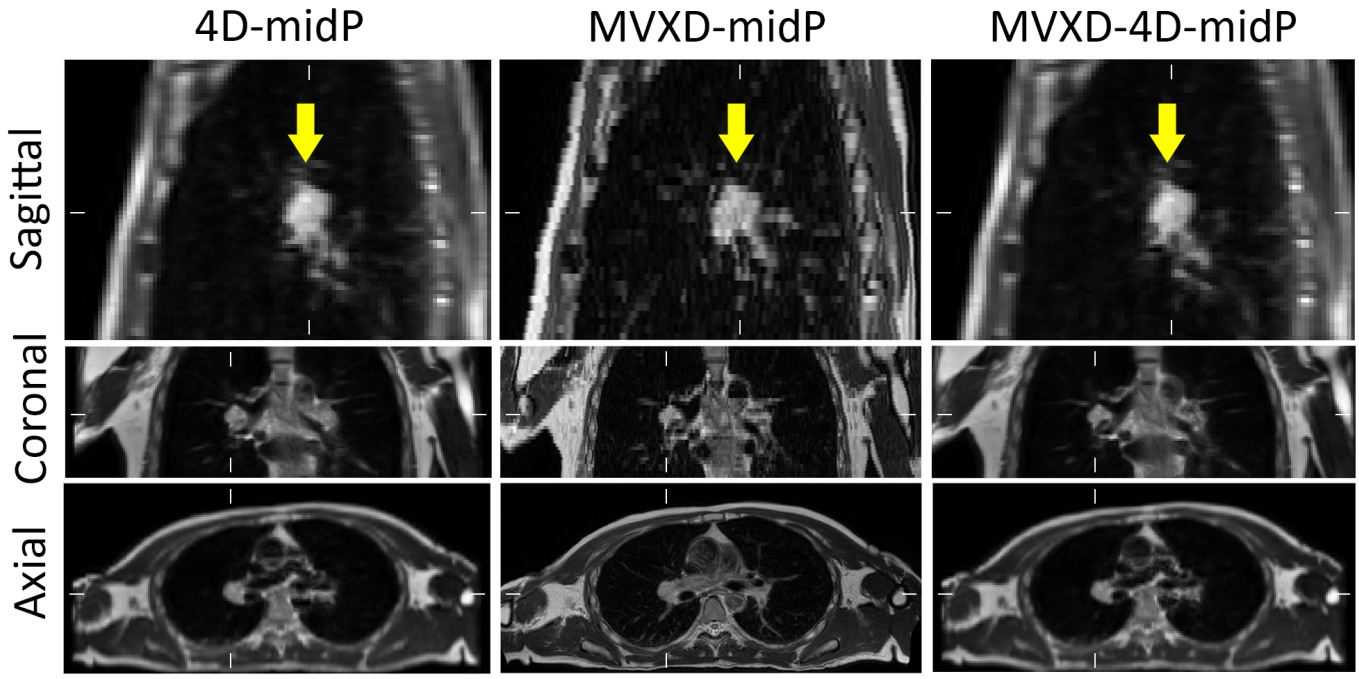

Fig. 4: Example patient comparison of midP images, created using ADMIRE. The yellow arrows point to the tumor. The white ticks show where the planes intersect.

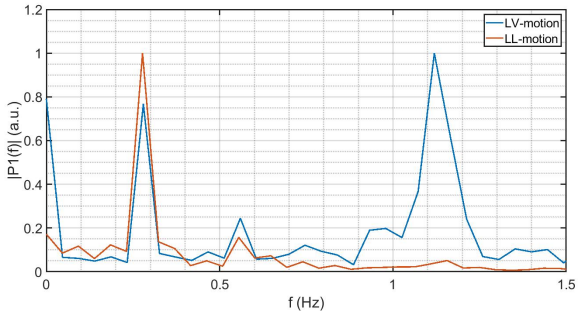

(a) Volunteer 5

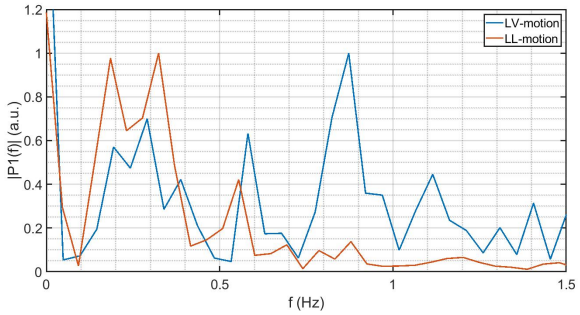

(b) Volunteer 6

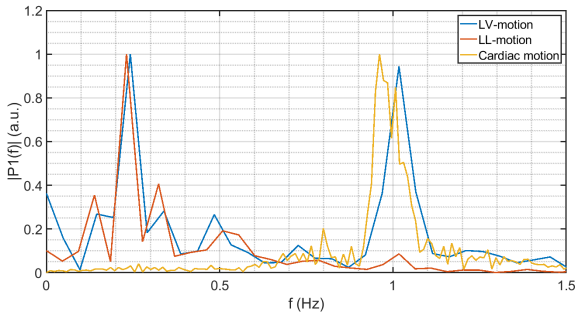

(c) Volunteer 7

Fig. 5: This figure shows the frequency spectrum of the motion in the cine images at the navigator location for three volunteers. It is clearly visible that the LV motion (blue) can be split into a respiratory component, comparable to the motion of the LL-interface (red), and a cardiac component, comparable to the signal measured for one volunteer with the PPU (yellow).

breathing artefact at the LL-interface was clearly visible for 2/1 volunteers in the LV-MVXD/LL-MVXD, while a moving heart artefact was visible for three volunteers in the LL-MVXD. For two volunteers a spot of hypointensity was seen in the liver in the LL-MVXD, at the location of the navigator. Such a hypointensity spot was not found at the LV in the LV-MVXD.

B. Evaluation midP

Fig. 4 shows midP images of one patient. It can be seen that image quality in the axial plane drastically increases in the MVXD-midP, when compared to the 4D-midP. Also in the sagittal plane, more details are visible in the MVXD-midP. The figure also shows that the MVXD-4D-midP is very similar to the 4D-midP.

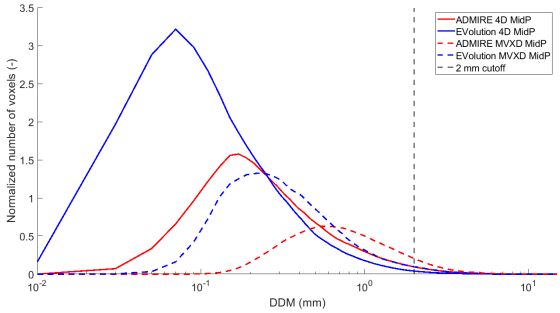

Fig. 6: DDM histograms for patients and volunteers combined. Note the logarithmic x-scale.

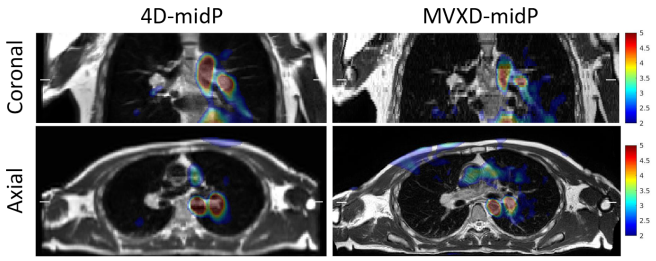

Fig. 7: The spatial distribution of the DDM for one patient. DDM values larger than 2 mm are shown.

1) DVF consistency: DVF consistency was determined by the DDM. The DDM distributions of the 4D-midPs are more shifted towards lower DDM values than those of the MVXD midPs (Fig. 6). The same can be said about the DDM values of midPs created by EVolution versus ADMIRE, midPs created by EVolution have lower DDM values. The same is reflected in the percentage of DDM values larger than 2 mm. Using EVolution, with the 4D-midPs 5% (volunteers) and 4% (patients) of DDM values are larger than 2 mm, and with the MVXD-midPs 23% (volunteers) and 9% (patients) are larger than 2 mm. Using ADMIRE, the percentages are 13% (volunteers) and 12% (patients) for the 4D-midPs, and 24% (both volunteers and patients) for the MVXD-midPs.

Fig. 7 shows the spatial distribution of the DDM for the same patient as is shown in Fig. 4. Elevated DDM values were found in areas with pulsatile flow such as the heart and blood vessels, and in areas with ghosting, such as the skin, arms and around the LL-interface.

2) Anatomical plausibility: Fig. 8 shows the absolute distance between the ground-truth translation and the actual translation of the tumor/LL-interface in the manual registrations for all different midPs. The mean/max motion amplitude in the 4D-midP was 10/27 mm. The 4D-midP (mean/max 0.3/1.0 for ADMIRE and 0.5/1.1 for EVolution) and the MVXD-4D-midP (mean/max 0.5/1.0 for ADMIRE and 0.6/2.0 for EVolution) have similar accuracy, while the MVXD-midP is less accurate (mean/max 0.5/1.5 for ADMIRE and 1.4/3.8 for EVolution). For the 4D-midP and the MVXD-4D-midP, ADMIRE and

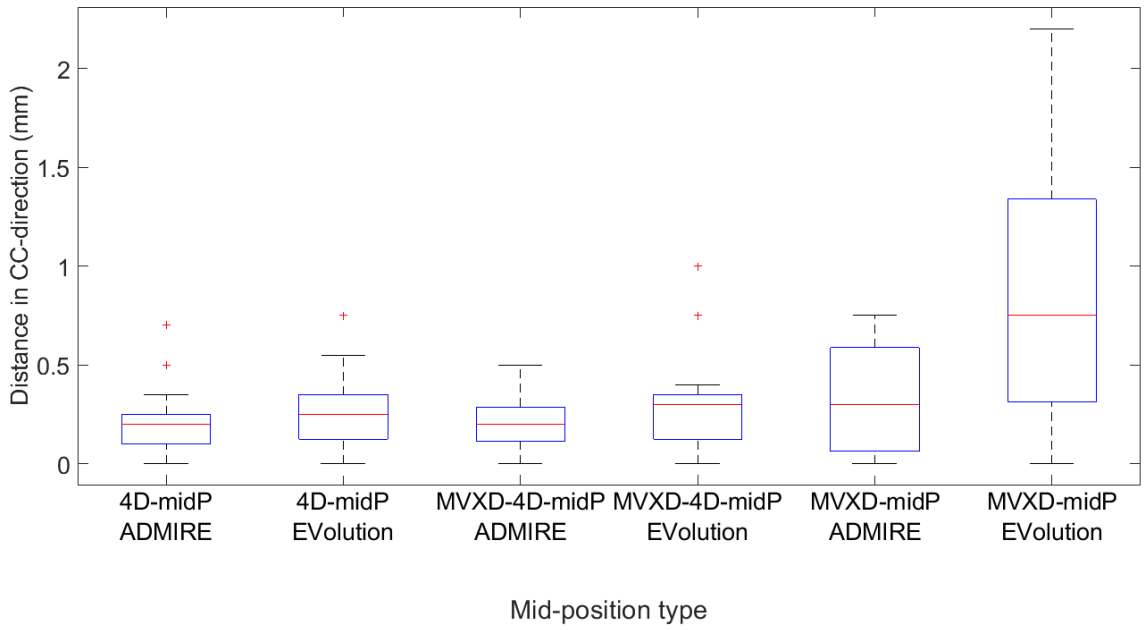

Fig. 8: Boxplot on absolute distance in CC-direction between the ground-truth midP and the actual midPs.

EVolution perform similarly, but for the MVXD-midP, EVolution is clearly less accurate than ADMIRE.

IV. Discussion

A. LV-MVXD

We have shown that placing a navigator on the LV results in motion detection of both a respiratory and a cardiac component, which is in agreement with previous research [13]. The motion of the LV contained both a respiratory and a cardiac component, which could be directly linked to the respiratory motion of the LL-interface and to the cardiac motion as measured with a pulse oximeter. Scanning with the navigator on the left ventricle halved the residual motion of the LL-interface and the LV with respect to no gating, indicating successful gating. Furthermore, the location of the LL-interface in the LV-MVXD was close to end-exhale, which shows that respiratory triggering was successfully applied.

Observers noticed that the LL-interface was generally sharper in the LL-MVXD, while for four out of five volunteers, the LV was sharper in the LV-MVXD. It was also observed that blood vessels and bronchi could be traced further into the lungs in the LV-MVXD compared to the LL-MVXD in one scan, showing that positive effects of LV-triggering are not limited to the heart itself. Many observed artifacts, such as the slice-to-slice contrast changes/low signal intensity in the heart region or the pulsation artifacts in large vessels also already occur in the original MVXD scan, so they are not caused by the adapted trigger setup.

For one volunteer, the triggering using the LV navigator was not optimal, which we already noticed during scanning. There was an almost continuous acquisition, where the heart rhythm was ignored, and even the respiratory motion was partly ignored. The results for this volunteer were not excluded in this research, and therefore had a negative impact on the results. For example, the residual motion with LV triggering was very high, and the scan quality was very low - this was the only scan where the LV-quality in the LV-MVXD was scored lower than in the LL-MVXD of the same volunteer. This shows that more research has to be done on optimally placing the navigator. The quality of the navigator signal will depend on the anatomy and heartbeat of the individual patient, which makes a uniform placement approach suboptimal. Fortunately suboptimal gating can be noticed immediately during scanning, so when the triggering is not successful, the acquisition can be stopped and the LL-MVXD can be acquired instead.

Surprisingly, average scan time of the MVXD increased with only 1% when changing from LL-navigation to LV-navigation. This could mean that the choice of gating window resulted in less strict respiratory triggering, which was compensated by additional constraints due to cardiac triggering, resulting in a similar duty cycle. This hypothesis is further supported by the fact that the LL-interface was usually scored worse in the LV-MVXD compared to the LL-MVXD, suggesting that respiratory triggering was less strict.

B. MVXD-based mid-position

Combining the MVXD and the 4D-MRI scans resulted in midP images with drastically higher resolution than the midP images purely based on the 4D-MRI. Structures are easier to recognize and delineate in the MVXD-midP.

The DVF consistency reduces when introducing the MVXD into midP calculation, which is probably caused by contrast differences between the scans. However, this reduced DVF consistency happens in areas with pulsatile flow, where the the scans itself are already less reliable, or in the skin, which is an area that is less relevant for delineation purposes. Furthermore,

the MVXD-4D-midP was very similar to the 4D-midP, which leads to the conclusion that the DVFs with the MVXD as reference were good enough to create a reliable midP image.

The manual registrations showed that structures in the 4D-midP and MVXD-4D-midP (for patients the tumors, for volunteers the LL-interface) were close to where they would theoretically be located based on the 4D-MRI alone. In these cases, the absolute distance between the actual and ground-truth translations were almost always smaller than 1 mm, which was the precision of the manual registrations. When using ADMIRE the MVXD-midP showed slightly less anatomical plausibility, but when using EVolution the anatomical plausibility reduced a lot.

Using this high-quality midP could improve treatment planning. A treatment based on a midP can be combined with trailing to reduce radiation margins even more [21]. With trailing, the treatment beam position is corrected for baseline drift, which is the slow drift of the tumor over multiple respiratory cycles. The beam follows the time-averaged tumor-position during delivery.

A downside of including the MVXD scan in midP calculations, is the impact on the workflow, since this requires acquisition of the MVXD scan, extending the preparation time before treatment can start. A possible solution for this would be to acquire the MVXD scan once on the MR-sim, and acquiring only the 4D-MRI daily on the MR-linac. However, this would negatively impact DVF accuracy, due to different patient positioning and slight changes in organ shape and position. The extend of this impact should be further investigated.

Using a method close to the method described in this thesis, it would be possible to warp the MVXD images to each respiratory phase of the 4D-MRI separately, to create a 4D-MRI with higher resolution, similar to the method described by Freedman *et al.* [22]. However, the reliability of such a 4D-MRI would be questionable in this case, since the individual registrations of the MVXD to the 4D-MRI are less reliable than 4D-MRI to 4D-MRI registrations, as shown by the DDM analysis. When creating a MVXD-based midP image, these errors partially cancel out, but when a high resolution 4D-MRI is made using a MVXD scan, there is only a single registration underlying each created 4D-phase, which introduces a large uncertainty.

Further research should focus on making LV-MVXD based midP images, as well as testing compatibility of the MVXD scan with MR-linac systems. The LV-MVXD should also be tested on patient volunteers, to investigate tumor visibility in the LV-MVXD, and midP images based on the LV-MVXD.

V. Conclusion

Placing the navigator in a triggered MRI on the left ventricle allows for cardiorespiratory triggering, which results in higher image quality in the heart region compared to respiratory triggering only. Furthermore, including a respiratory triggered MRI in mid-position calculations is feasible, and results in mid-position images with much higher quality than mid-position images based on purely 4D-MRI.

References

[1] P. J. Keall et al. “The management of respiratory motion in radiation oncology report of AAPM Task Group 76”. In: *Med Phys* 33.10 (2006), pp. 3874–3900.

[2] D. A. Low et al. “A method for the reconstruction of four-dimensional synchronized CT scans acquired during free breathing”. In: *Med Phys* 30.6 (2003), pp. 1254–1263.

[3] B. Stemkens, E. S. Paulson, and R. H. N. Tijssen. “Nuts and bolts of 4D-MRI for radiotherapy”. In: *Phys Med Biol* 63.21 (2018), 21TR01.

[4] C. Paganelli et al. “MRI-guidance for motion management in external beam radiotherapy: current status and future challenges”. In: *Phys Med Biol* 63.22 (2018), 22TR03.

[5] J. Olsen, O. Green, and R. Kashani. “World’s First Application of MR-Guidance for Radiotherapy”. en. In: *Mo Med* 112.5 (2015), pp. 358–360.

[6] B. W. Raaymakers et al. “First patients treated with a 1.5 T MRI-Linac: clinical proof of concept of a high-precision, high-field MRI guided radiotherapy treatment”. en. In: *Phys Med Biol* 62.23 (2017), pp. L41–L50.

[7] S. Kumar et al. “Magnetic resonance imaging in lung: a review of its potential for radiotherapy”. In: *The British Journal of Radiology* 89.1060 (2016), p. 20150431.

[8] P. Giraud and A. Houle. “Respiratory Gating for Radiotherapy: Main Technical Aspects and Clinical Benefits”. In: *ISRN Pulmonology* 2013 (2013), p. 519602.

[9] J. W. H. Wolthaus et al. “Reconstruction of a time-averaged midposition CT scan for radiotherapy planning of lung cancer patients using deformable registration”. en. In: *Med Phys* 35.9 (2008), pp. 3998–4011.

[10] J. N. Freedman et al. “Super-resolution T2-weighted 4D MRI for image guided radiotherapy”. In: *Radiother Oncol* 129.3 (2018), pp. 486–493.

[11] T.N. van de Lindt et al. “MRI-guided mid-position liver radiotherapy: Validation of image processing and registration steps”. In: *Radiotherapy and Oncology* 138 (2019), pp. 132–140.

[12] J. Pomp et al. “Sarcoma of the Heart Treated with Stereotactic MR-Guided Online Adaptive Radiation Therapy”. In: *Case Rep Oncol* 14.1 (2021), pp. 453–458.

[13] K. Nehrke and D. Manke. “Advanced Navigator Techniques”. In: *IJBEM* 2.2 (2000), pp. 248–254.

[14] K. Keijnemans et al. “Simultaneous multi-slice accelerated 4D-MRI for radiotherapy guidance”. In: *Physics in Medicine & Biology* 66.9 (2021), p. 095014.

[15] J. G. Pipe. “Motion correction with PROPELLER MRI: application to head motion and free-breathing cardiac imaging”. In: *Magn Reson Med* 42.5 (1999), pp. 963–969.

[16] Yu L. Liu et al. “A monitoring, feedback, and triggering system for reproducible breath-hold MR imaging”. In: *Magnetic Resonance in Medicine* 30.4 (1993), pp. 507–511.

[17] O. Akdag et al. “Feasibility of free breathing real-time cine-MRI for MR-guided Cardiac Radioablation on the Unity MR-linac”. In: *Proc. Intl. Soc. Mag. Reson. Med.* 29 Abstract 4014. 2021.

[18] B. Denis de Senneville et al. “EVolution: an edge-based variational method for non-rigid multi-modal image registration”. In: *Phys Med Biol* 61.20 (2016), pp. 7377–7396.

[19] Z. H. Saleh et al. “The distance discordance metric-a novel approach to quantifying spatial uncertainties in intra- and inter-patient deformable image registration”. In: *Phys Med Biol* 59.3 (2014), pp. 733–746.

[20] K. K. Brock et al. “Use of image registration and fusion algorithms and techniques in radiotherapy: Report of the AAPM Radiation Therapy Committee Task Group No. 132”. In: *Med Phys* 44.7 (2017), e43–e76.

[21] M. F. Fast et al. “Tumor Trailing for Liver SBRT on the MR-Linac”. In: *International Journal of Radiation Oncology*Biology*Physics* 103.2 (2019), pp. 468–478.

[22] J. N. Freedman et al. “T2-Weighted 4D Magnetic Resonance Imaging for Application in Magnetic Resonance-Guided Radiotherapy Treatment Planning”. In: *Invest Radiol* 52.10 (2017), pp. 563–573.

Evaluatie van LV-gated MVXD beelden voor long.

Vrijwilliger nummer: MR21V3 (Let op: de vragenlijst is verschillend per vrijwilliger, dus gebruik steeds de vragenlijst die bij de betreffende vrijwilliger hoort)
Beoordelaar:

Deel I: Het vergelijken van de beeldkwaliteiten.

De MVXD beelden zouden gebruikt kunnen worden voor long radiotherapie. Houd dit in gedachten bij het beantwoorden van de vragen van deel 1. Bij patiënten zal het FOV aangepast worden zodat de volledige long in beeld is.

Vraag 1a: De algemene beeldkwaliteit vind ik:

	Niet-bruikbaar	Slecht	Ok	Goed
MVXD A				
MVXD B				

Vraag 1b: De beeldkwaliteit van de volgende aanzichten van de **MVXD A** beelden vind ik:

	Niet-bruikbaar	Slecht	Ok	Goed
Axiaal				
Coronaal				
Sagittaal				

Vraag 1c: De beeldkwaliteit van de volgende aanzichten van de **MVXD B** beelden vind ik:

	Niet-bruikbaar	Slecht	Ok	Goed
Axiaal				
Coronaal				
Sagittaal				

Vraag 1e: Indien er artefacten aanwezig waren in bepaalde beelden, beschrijf hieronder welke artefacten gevonden werden in deze beelden:

MVXD A	**MVXD B**

Deel II: Het vergelijken van de beeldkwaliteiten voor het beoordelen van de target en OAR

Zorg dat bij het beantwoorden van de vragen in deel II in Volumetool, de volgende window-level instelling worden toegepast:

MVXD A: Window = 1847.350, level = 1062.775
MVXD B: Window = 1835.300, level = 1055.750

Vraag 2: Ik kan de volgende structuren beter afgrenzen op een van de scans.

Structuur	Beter op **MVXD A**	Gelijk	Beter op **MVXD B**	Niet zichtbaar / niet in FOV
Wervelkolom				
Trachea				
Linker en rechter bronchus (hoofdtak)				
Aorta				
Hart				
Oesofagus				
Lever				

Vraag 3: Beschouw de verschillende vlakken apart. Scroll door de beelden. De **lever-long overgang** is scherper op een van de scans.

Vlak	Scherper op **MVXD A**	Gelijk	Scherper op **MVXD B**
Coronaal			
Sagittaal			

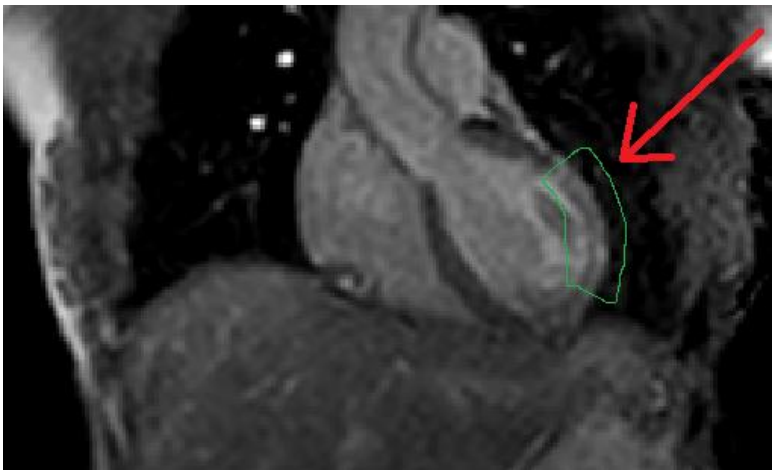

Figuur 1: *Afbeelding van de te beoordelen hartwand.*

Vraag 4a: Kijk in het **coronale** vlak. Scroll door de beelden. Het deel van de **hartwand** zoals aangegeven op de screenshot hierboven (Fig. 1) is scherper op een van de scans.

Scherper op **MVXD A**	Gelijk	Scherper op **MVXD B**

Figuur 2: *Afbeelding van de te beoordelen hartwand.*

Vraag 4b: Kijk in het **sagittale** vlak. Scroll door de beelden. Het deel van de **hartwand** zoals aangegeven op de screenshot hierboven (Fig. 2) is scherper op een van de scans.

Scherper op **MVXD A**	Gelijk	Scherper op **MVXD B**

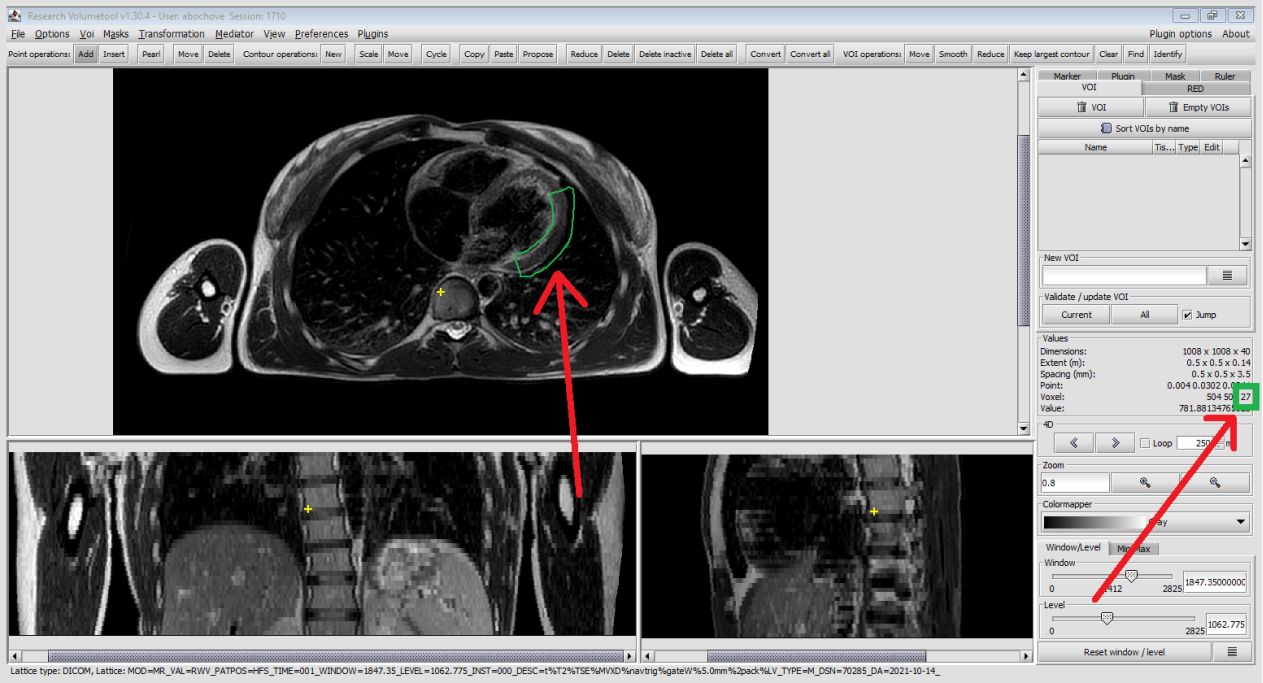

Figuur 3: *Screenshot van Volumetool, geeft aan waar de nummering gevonden kan worden (in dit geval plak 27) en welk deel van de hartwand beoordeeld moet worden.*

Vraag 5: Kijk in het **axiale** vlak. Kijk in plakken 16-32 (houd de nummering van Volumetool aan, Fig. 3). Onderzoek twee structuren in iedere plak opnieuw, zoals beschreven staat in de tabel.

	Het deel van de **hartwand** zoals aangegeven op de screenshot hierboven (Fig. 3).		De **oesofagus**.	
	Dit is scherper op **MVXD A**	Dit is scherper op **MVXD B**	Dit is scherper op **MVXD A**	Dit is scherper op **MVXD B**
Slice 16				
Slice 17				
Slice 18				
Slice 19				
Slice 20				
Slice 21				
Slice 22				
Slice 23				
Slice 24				
Slice 25				
Slice 26				
Slice 27				
Slice 28				
Slice 29				
Slice 30				
Slice 31				
Slice 32				

Deel III: Algemene vragen

Vraag 6: Wat zijn pluspunten en minpunten van de beelden?

	Pluspunten	Minpunten
MVXD A		
MVXD B		

Vraag 7: Heeft u nog overige opmerkingen?

In dit onderzoek heb ik gewerkt aan MRI beelden die gebruikt worden bij het bestralen van tumoren in longen.
Als een patiënt ademt, zal een tumor in de longen altijd meebewegen. Momenteel wordt de bestraling zo gedaan dat de tumor altijd geraakt wordt, waar de patiënt ook zit in de ademhaling. Echter, hierdoor wordt er ook altijd gezond weefsel geraakt door de straling, en dat kan schadelijk zijn. Als oplossing hiervoor wordt er uitgezocht wat de *gemiddelde positie* van de tumor is, en die locatie wordt dan bestraald. Op deze manier wordt de tumor gemiddeld gezien overal bestraald. Om de gemiddelde positie van een tumor te kunnen vinden, moet er een afbeelding zijn van de *gemiddelde anatomie* van een patiënt, dit heet een *mid-positie* afbeelding.
Een mid-positie afbeelding kan gemaakt worden aan de hand van een *4D-scan*. Dat is een scan waarbij er verschillende 3D-scans worden gemaakt in verschillende *ademhalingsfases.* Zo krijg je een 3D-scan als de patiënt heeft uitgeademd, als deze heeft ingeademd, en in verschillende fases ertussenin. Omdat een 4D-scan informatie bevat over de hele ademhalingscyclus, kan deze gebruikt worden om een mid-positie afbeelding te maken.
Ik heb gewerkt met een *4D-MRI* scan. De resolutie van de mid-positie afbeeldingen op basis van de 4D-MRI is niet heel goed. Daarom heb ik de 4D-MRI scan gecombineerd met een andere MRI-scan die een veel hogere resolutie heeft. Op deze manier kan er een mid-positie afbeelding worden gemaakt met een hogere resolutie. Er zijn 13 patiënten gescand met de 4D-MRI en de hoge resolutie scan, en ik heb 2 vrijwilligers gescand. Ik heb deze scans gebruikt om mid-positie beelden te maken, en hieruit bleek dat de kwaliteit van de scans flink toeneemt als de hoge resolutie scan wordt gebruikt. Dit is te zien in figuur 4 (links is alleen met de 4D-MRI, midden is met de hoge resolutie scan gecombineerd).
Deze MRI-scan met hoge kwaliteit wordt opgenomen terwijl de patiënt normaal ademt, maar het scannen gebeurt alleen op het moment dat de patiënt heeft uitgeademd. Hierdoor ontstaat er een scherp beeld, waar ademhaling weinig negatieve invloed op de kwaliteit heeft. Echter, met de beweging van het hart is geen rekening gehouden, dus rond het hart is de beeldkwaliteit minder.
Ik heb de scan aangepast zodat deze niet alleen rekening houdt met de ademhaling, maar ook met hartbeweging. Dit heb ik uitgetest op 5 vrijwilligers, en het blijkt goed te werken, de kwaliteit rond het hart wordt beter na deze aanpassing. Dit is te zien in figuur 3 (links is met compensatie voor ademhaling, rechts met compensatie van ademhaling en hartbeweging). De gemaakte MRI-scans zijn beoordeeld door een radioloog en door twee radiotherapeut-oncologen, en zij vonden ook dat de kwaliteit rond het hart beter was nadat de scans waren aangepast.
Met dit onderzoek heb ik aangetoond dat het zeer nuttig kan zijn om de 4D-MRI te combineren met de hogere kwaliteit scan, om een mid-positie afbeelding te krijgen met een hogere resolutie. Verder heb ik laten zien dat de scan kan worden aangepast zodat er ook rekening gehouden kan worden met hartbewegingen, wat een positieve invloed heeft op de beeldkwaliteit.